Effect of local Peregrine soliton emergence on statistics of random waves in the one-dimensional focusing nonlinear Schrödinger equation

Alexey Tikan *

University of Lille, UMR 8523-PhLAM-Physique des Lasers Atomes et Molecules, F-59000 Lille, France

(Received 4 June 2019; revised manuscript received 27 October 2019; published 14 January 2020)

The Peregrine soliton is often considered as a prototype of rogue waves. After recent advances in the semiclassical limit of the one-dimensional focusing nonlinear Schrödinger equation [M. Bertola and A. Tovbis, Commun. Pure Appl. Math. **66**, 678 (2013)] this conjecture can be seen from another perspective. In the present paper, connecting deterministic and statistical approaches, we numerically demonstrate the effect of the universal local emergence of Peregrine solitons on the evolution of statistical properties of random waves. Evidence of this effect is found in recent experimental studies in the contexts of fiber optics and hydrodynamics. The present approach can serve as a powerful tool for the description of the transient dynamics of random waves and provide new insights into the problem of the rogue waves formation.

DOI: 10.1103/PhysRevE.101.012209

I. INTRODUCTION

Ocean waves of extremely high amplitude appear more often than it is predicted by linear theory [1,2]. Such waves are known as freak or rogue waves (RWs). One of the first examples of directly recorded RWs is the New Year wave that crashed onto the Draupner platform in the North Sea in 1995 [3]. The measured wave height was 25.6 m (trough to crest), while the significant wave height (four standard deviations of the surface elevation) was approximately 12 m. Waves of such amplitude unconditionally represent a great danger to mariners. Therefore, understanding the nature of RWs and predicting their emergence are problems of paramount importance in physics [1,4,5].

The first water tank experiment aiming to demonstrate the emergence of RWs in well-controlled laboratory conditions is reported in Ref. [6]. The authors studied the nonlinear dynamics of unidirectional waves on the surface of the deep water. In order to mimic the real sea state, a spectrum having a particular asymmetric shape and delta-correlated phases of every Fourier component was used to generate the random initial conditions. This spectrum was found empirically during the measurements obtained in the North Sea in the 1960s known as the Joint North Sea Wave Project (JONSWAP) [7]. According to the central limit theorem, a superposition of a large number of independent Fourier modes leads to the Gaussian distribution for the surface elevation. Therefore, the modulus of the envelope is described by the Rayleigh distribution and the modulus square of the envelope by the exponential distributions [8]. A random wave that has these statistical properties is often referred to as a partially coherent wave. The authors demonstrated that the distribution of the partially coherent waves deviates from the Gaussian during the propagation in the water tank. This deviation signifies that the probability of extreme events to emerge is increased. Moreover, the rate of the deviation strongly depends on the parameters of the initial conditions and the propagation distance.

This remarkable observation is in good agreement with numerical simulations of different hydrodynamic models [10]. The leading-order model that can be applied to unidirectional gravity waves on the surface of deep water is the one-dimensional (1D) focusing nonlinear Schrödinger (NLS) equation [2,11–14]. The NLS equation is a universal equation that describes the evolution of nonlinear dispersive waves under the assumption of a slowly varying envelope and a small wave steepness. Besides deep water waves this model governs at the leading order dynamics of electromagnetic waves in a single-mode fiber [15] and many other physical systems [16]. The NLS equation became a subject of a broad interest after the proof of its integrability with the inverse scattering transform (IST) method [17]. It is important to point out that the applicability of envelope models to random water waves is a subject of ongoing debates, but there are convincing arguments provided in Refs. [14,18–20].

The presence of solitonic solutions follows directly from the integrability of the 1D focusing NLS equation. A family of solitons on the finite background plays an important role in the context of RWs. It is represented by solitons of a certain amplitude interacting with a plane wave. The dynamics of such solutions depends on the ratio between the amplitude of the soliton and the level of the plane wave background. There are three well-known members of this family: the Akhmediev breather [21], Kuznetsov-Ma soliton [22,23], and Peregrine soliton (PS) [24]. Solitons of the finite background are widely considered as prototypes of the RWs [13,25,26]. The PS (see Fig. 1) is localized both in space and in time. This property coincides well with the well-known characteristic of a RW: it appears out of nowhere and disappears without a trace. The particular importance of the PS in this context is highlighted in Ref. [27]. Its emergence is usually related to the mechanism of the modulation instability of a perturbed plane wave (also known as the Benjamin-Feir instability) [28].

* alexey.tikan@univ-lille.fr

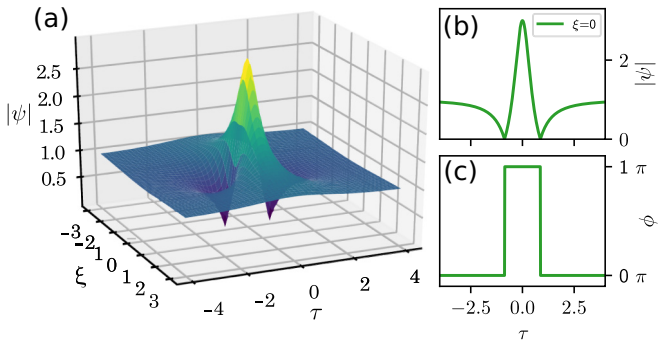

FIG. 1. Evolution of the PS. (a) Spatiotemporal diagram of $|\psi|$ plotted according the analytical formula [9]. (b) Cross section at $\xi = 0$. (c) Corresponding phase.

The presence of the local PSs in the spatiotemporal evolution of the partially coherent wave in the 1D focusing NLS governed systems is an experimentally verified fact [29–31]. However, the modulation instability cannot be considered as a dominating mechanism in this case. Recent advances in the semiclassical (zero-dispersion) limit of the focusing NLS equation revealed another fundamental mechanism that *universally* leads to the emergence of local PSs. Self-focusing dynamics of a smooth single hump, in the case when nonlinearity significantly dominates dispersion, inevitably leads to a gradient catastrophe. It was proved in Ref. [32] and experimentally verified in Ref. [33] that the structure which appears as a regularization of the gradient catastrophe asymptotically tends to the PS. Since the partially coherent wave can be seen as a set of independent humps at the early stage of the nonlinear propagation, the gradient catastrophe regularization mechanism is expected to play an important role in its evolution.

In the present article, we numerically demonstrate the influence of the universal local emergence of the PSs on statistical characteristics of partially coherent waves. This link between deterministic and statistical approaches to the RWs' formation problem reveals that the position of the most probable emergence of local PSs coincides well with the maximum of the fourth-order statistical moment (kurtosis), employed here as a measure of the deviation from Gaussian statistics. Using analytical results obtained in the semiclassical approximation, we show that this position can be effectively predicted in a wide range of parameters.

II. SEMICLASSICAL LIMIT OF NLS: UNIVERSAL EMERGENCE OF LOCAL PEREGRINE SOLITONS

The emergence of the PS out of smooth rapidly decaying initial conditions is proved in the semiclassical (or zero-dispersion) limit of the 1D NLS equation. The zero-dispersion limit implies that the parameter ϵ in the 1D NLS equation (1) tends to zero, so the nonlinearity significantly exceeds the dispersion.

We write the 1D focusing NLS equation in the following way:

$$i\epsilon\frac{\partial\psi}{\partial\xi} + \frac{\epsilon^2}{2}\frac{\partial^2\psi}{\partial\tau^2} + |\psi|^2\psi = 0, \tag{1}$$

where ξ and τ are spatial and temporal variables, respectively, $\epsilon = \sqrt{L_{NL}/L_D}$ with L_{NL} the typical nonlinear and L_D typical linear lengths, respectively [15]. In terms of variables adopted in optics it is written as follows: $\epsilon = \sqrt{|\beta_2|/\gamma P_0 T_0^2}$, where β_2 is the group velocity dispersion coefficient, γ the third-order nonlinearity coefficient, $P_0 = \frac{1}{T}\int_0^T < |\psi(\tau,0)|^2 > d\tau$ is the ensemble-averaged number of particles, and T_0 is typical coherence time inversely proportional to the spectral width. Parameter ϵ is exactly the inverse of the Benjamin-Feir index widely used in hydrodynamics [10].

Let us apply the so-called Madelung transformation [34,35]:

$$\psi(\xi,\tau) = \sqrt{\rho_m(\xi,\tau)}e^{i\phi(\xi,\tau)/\epsilon}, \quad u(\xi,\tau) = \phi_\tau(\xi,\tau), \tag{2}$$

where $\sqrt{\rho}$ is the wave amplitude and u the instantaneous frequency. The 1D NLS Eq. (1) can be expressed as a system of equations by separation of real and imaginary parts:

$$\rho_\xi + (\rho u)_\tau = 0, \tag{3}$$

$$u_\xi + uu_\tau - \rho_\tau + \frac{\epsilon^2}{4}\left[\frac{\rho_\tau^2}{2\rho^2} - \frac{\rho_{\tau\tau}}{\rho}\right]_\tau = 0. \tag{4}$$

In this form, the meaning of the introduced variables can be easily understood. Indeed, the first equation is similar to a continuity equation, with ρ fluid density and u flow velocity field. Together with the second one these equations are an analog of Euler equations for dispersive hydrodynamics but with a negative pressure $p = -\rho^2/2$.

The last term in Eq. (4) is proportional to ϵ^2, and therefore it can be neglected at the early stage of the propagation. As is shown in Refs. [32,36], the propagation of smooth rapidly decaying initial conditions is described by Eqs. (3) and (4) until a certain distance where the gradients of ρ or u become (infinitely) large. This distance is called the point of the *gradient catastrophe*. For the reduced set of equations, the problem is ill-posed, and the full system has to be considered. The way to describe solutions in the vicinity of the gradient catastrophe point is to use benefits of the semiclassical approximation in the IST method. This is performed by Bertola and Tovbis [32]. They found that the gradient catastrophe is regularized by *universal* appearance of a local coherent structure which asymptotically tends to the PS. Here the term universal is used to underline that the Bertola-Tovbis scenario does not depend on the exact shape, chirp, or solitonic content of the smooth initial conditions. Similar dynamics is observed in the 1D NLS equation with linear damping and a Gaussian driving, as well as a discrete analog of the NLS equation [37,38].

More explicitly the theory discussed above predicts at the leading order that the point of PS emergence is given by the following expression:

$$\xi_m = \xi_c + C\epsilon^{4/5}, \tag{5}$$

where ξ_m is the maximum compression point, $\xi_c = 1/2$ is the point of gradient catastrophe in the case of absence of a chirp, and $C = 0.955262458\ldots$ is a universal constant.

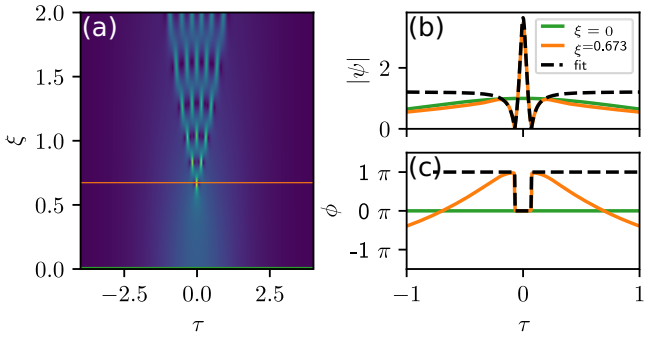

FIG. 2. Regularization of the gradient catastrophe by local emergence of the PS. Parameter ϵ in the simulation is 1/10. (a)–(c) Spatiotemporal diagram, amplitude, and phase cross section, respectively, at the maximum compression point. The 10sech(τ) function is taken as an initial condition. The black dashed line represents a fit of the local PS with the analytical formula (6). The maximum compression point in the simulation occurs at the distance $\xi = 0.673$, while the distance predicted by expression (5) is 0.6514.

The structure that emerges is approximated as

$$|\psi(\tau, \xi_m)| = a_0\left[1 - \frac{4}{1 + 4a_0^2(\tau/\epsilon)^2}\right][1 + O(\epsilon^{1/5})], \quad (6)$$

which coincides with the formula of PS if $\epsilon \ll 1$.

This result is verified in fiber optics experiments with isolated light pulses [33]. Fiber optics experiments demonstrated that this scenario can be observed far beyond the formal range of applicability of the semiclassical limit of the 1D NLS. Regularization of the gradient catastrophe by emergence of a coherent structure that is *locally* fitted by the PS is observed up to $\epsilon \approx 0.45$.

We demonstrate the PS's emergence with the following example. Consider initial conditions in the form of exact N solitons solution, $\psi(0, \tau) = \mathrm{sech}(\tau)$ with coefficient $\epsilon = 1/N$ in Eq. (1) [Figs. 2(b) and 2(c), green line $N = 10$]. The spatiotemporal diagram of its evolution in the 1D focusing NLS equation [Fig. 2(a)] shows that the self-focusing dynamics leads to the maximum compression point at $\xi = 0.673$. According to semiclassical theory the point of the maximum compression occurs at $\xi = 0.6514$. The cross sections [Fig. 2(b)] show that the coherent structure that emerges is locally similar to the PS including the characteristic phase jump of π [Fig. 2(c)]. This is in a good agreement with the exact analytical expression (6) depicted with the black dashed line in Figs. 2(b) and 2(c).

III. LOCAL PEREGRINE SOLITONS IN INTEGRABLE TURBULENCE

Evolution of random waves in a system governed by an integrable model may be considered in the framework of integrable turbulence. The concept of integrable turbulence was introduced by Zakharov [39]. In the context of the 1D focusing NLS equation there are two kinds of initial conditions that are widely studied: a quasimonochromatic wave with a small random perturbation (condensate) [25,40–43] and the partially coherent wave [6,10,29,30,44–46]. A transition between these two cases is studied as well using the numerical IST spectra computation [47,48].

In the first case, the underlying mechanism is well understood: the monochromatic wave is unstable towards a small perturbation, and, therefore, spatiotemporal dynamics is driven by modulation instability. Recent advances in the perturbation approach to this problem allowed researchers to solve exactly the direct and inverse problems for the condensate with a small periodic noise [49,50]. However, it has been shown that the evolution of the condensate does not lead to a more frequent emergence of extreme events at the stationary state than is predicted by the central limit theorem [40].

Discussion about a mechanism that drives the partially coherent wave dynamics can be found in Ref. [51]. The authors point out that structures locally similar to the PS are often found in the numerical simulations and experimental measurements of the partially coherent wave propagation. Recent water tank experiments confirm the observation [30,31]; see also Ref. [52].

The definition of the partially coherent wave used in this article is the following:

$$\psi(\xi, \tau) = \sum_k a_k(\xi) \exp^{\frac{2\pi i}{T} k\tau} \text{ with } k \in \mathbb{Z}, \quad (7)$$

where $a_k(0) = |a_{0k}|e^{i\phi_{0k}}$ is a kth Fourier component with a uniformly distributed random phase $\phi_{0k} \in [-\pi, \pi]$ and Gaussian-shaped amplitude squares with the full width at half maximum 1/2. This way to introduce the partially coherent wave guaranties the periodical boundary conditions with the period T.

Figure 3(b) shows a numerically generated spatiotemporal diagram of the partially coherent wave propagated in the NLS system with $\epsilon = 0.2$. The average number of particles of the partially coherent wave P_0 is set to 1 as well as the typical initial hump's duration. Due to the focusing nature of Eq. (1), partially coherent initial conditions can be considered at the early stages of propagation as a set of independent humps, which also follows from the diagram. We also see that if a hump exceeds a certain limit, its dynamics inevitably leads to the formation of a high-amplitude coherent structure. It was shown previously that such structures can be *locally* fitted by the PS [29,44]. Local PSs that emerged out of initial humps are highlighted by white rectangles. Figure 3(d) demonstrates cross sections of the spatiotemporal diagram at $\xi = 0$ (green) and 0.366 (orange). As we see, each local hump produces at the first step a single spike during the propagation. The maximum compression point of the spike depends on the initial parameters of each isolated hump. Around the point $\tau = 2$ we observe the spike at its maximum compression. The zoomed window in the center shows the fit with the analytical formula of the PS (black dashed line). Remarkably, emergence of the PS out of a hump which exceeds a certain critical parameter was predicted in Ref. [27] but in the presence of a continuous background.

Statistical properties of this system such as a spectrum or probability density function (PDF) evolve together with ξ. The evolution is found numerically using an ensemble of 10 000 realizations of the partially coherent waves obtained

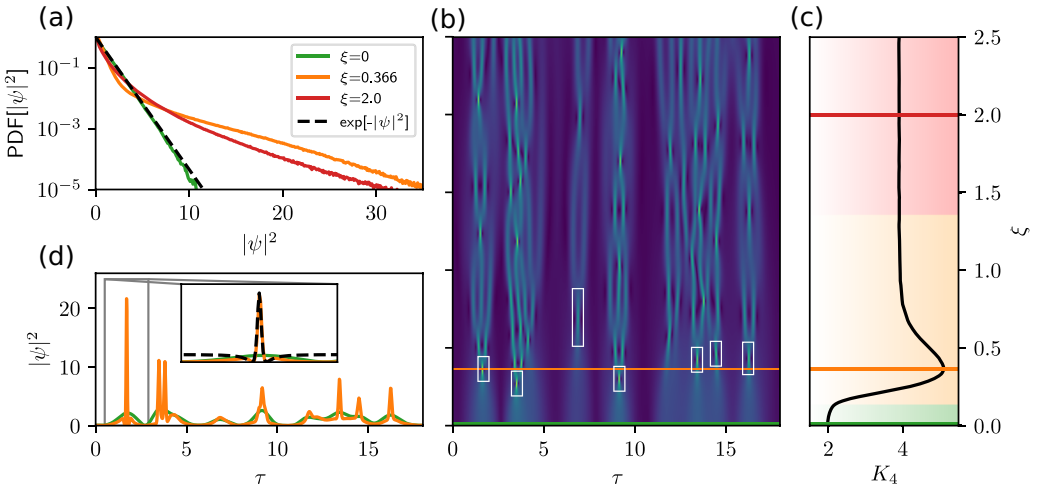

FIG. 3. Numerical simulations of a partially coherent wave propagation in the focusing NLS system. (a) Probability density function of $|\psi|^2$ at three different propagation distances: $\xi = 0$ (green), 0.366 (orange), and 2 (red). The dashed black line corresponds to $\exp(-|\psi|^2)$. (b) Spatiotemporal diagram of $|\psi|$. White boxes highlight the coherent structures that appear out of initial humps and can be locally fitted with the PS. (c) Evolution of the kurtosis (black). Green, orange, and red lines correspond to $\xi = 0$, 0.366, and 2. The kurtosis and the probability density function are computed over 10 000 realizations of the partially coherent wave similar to one depicted in panel (b). (d) $|\psi|^2$ profile at two values of $\xi = 0$, 0.366 (colors are preserved). Inset plot demonstrates a fit of the high-amplitude event with the exact formula of the PS. In all the simulations the value of ϵ is 0.2.

by randomizing a phase of each Fourier component. Every realization is done in a numerical box of 2^{13} points which covered 80 normalized time units. The PDF of a partially coherent wave propagating in a system governed by the 1D focusing NLS equation was shown to deviate from the exponential forming L-shaped heavy-tailed distribution [44] [see Fig. 3(a)]. It signifies that the probability of the high-amplitude events to appear increases during the nonlinear propagation. This deviation is often characterized by a normalized fourth-order moment also known as the kurtosis. In this paper we use the following definition of the kurtosis: $K_4 = \langle|\psi|^4\rangle/\langle|\psi|^2\rangle^2$, where $\langle\cdots\rangle$ stands for the ensemble averaging.

The evolution of the kurtosis can be divided into three parts [Fig. 3(c)]. The first one (green area) corresponds to an early stage of the evolution. In this case, the intensity profile does not experience significant changes, while the phase correlation occurs. The early stage of the evolution of kurtosis is fully described in the semiclassical limit [53]. Deviation of the theory in the vicinity of the rising slope was related to the occurrence of the gradient catastrophes in the dynamics of initial humps. The second part (orange area) has a well-defined *local maximum* (also called overshoot), which is not present in the defocusing case [45,54]. At this stage the dynamics of each local hump can still be studied separately from its neighbors. At the distance corresponding to the maximum of K_4 the probability to observe the RW is the highest. Moreover, according to Ref. [54], the maximum of K_4 corresponds to the maximum of the spectral width. The third part (red area) corresponds to the stationary state of the partially coherent wave dynamics. The description of the stationary state remains an open problem; however, a recent study demonstrated promising results in describing the stationary state of the modulation instability using a soliton gas concept [55].

IV. EFFECT OF LOCAL PEREGRINE SOLITONS ON THE EVOLUTION OF STATISTICAL CHARACTERISTICS

Validity of the semiclassical theory in a wide range of values of ϵ signifies that the scenario of regularization of the gradient catastrophe by emergence of a local PS due to its universality can have a trace in the dynamics of partially coherent waves. As we demonstrated, partially coherent initial conditions could be seen as a set of separated humps at the early stage of the nonlinear propagation. The form of the humps can be complex and irregular; however, the result of Bertola and Tovbis does not depend on the particular shape of initial conditions requiring it only to be smooth. Therefore, we expect that evolution of every individual hump having a value of ϵ_{loc} below a certain threshold will lead to the appearance of localized PS.

A partially coherent wave has a typical coherence time $T_h \sim 1/\Delta\nu$, where $\Delta\nu$ is a spectral width. Moreover, the distribution of amplitudes of the local humps has a maximum which depends on the average number of particles P_0. Therefore, we can conclude that the distribution of values of ϵ_{loc} locally computed for each hump will also have a certain maximum. The presence of a statistically most probable value of locally estimated ϵ_{loc} implies that there is a propagation distance at which the emergence of the PS is the most probable.

The probability distribution of a PS to appear as a function of ξ can be estimated numerically using Eq. (5). We generate the partially coherent initial conditions in the Fourier space according to the expression (7). The parameters of the numerical simulations are the same as the ones adopted in Sec. III. The values of ϵ_{loc} are estimated by numerically detecting each local hump in the initial conditions. In order to take into account only the humps that will produce a PS and contribute significantly to the statistics we put a threshold $|\psi(\tau, 0)|^2_{th} = 2.5P_0$ found empirically. We exclude double or

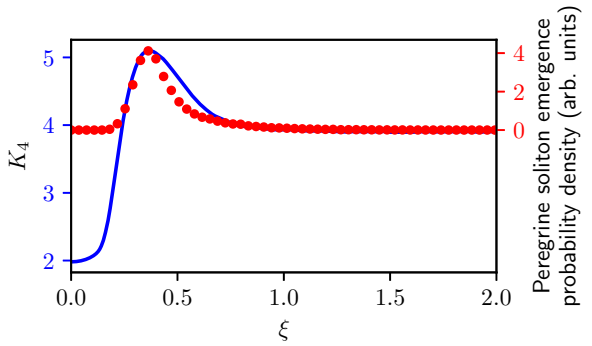

FIG. 4. Prediction of the maximum of the kurtosis using the Bertola-Tovbis approach. Comparison between the probability density of local PS soliton emergence point (red dot, right axis) and the kurtosis at different propagation distances (blue line, left axis). All parameters coincide with ones in Fig. 3.

multihump structures requiring the minimal distance between the considered peaks to be more than 2. The value of ϵ_{loc} for every initial hump satisfying the above criteria is estimated as follows:

$$\epsilon_{\text{loc}} = \epsilon/(T_{\text{loc}}\sqrt{P_{\text{loc}}}),$$

where $\epsilon = 0.2$, T_{loc} is the duration of the hump at the half maximum of amplitude and P_{loc} is the square of maximum value of the local hump amplitude. Further, we can apply Eq. (5) and find a distribution of the PS emergence substituting the value of ϵ_{loc} and renormalizing the distance for each detected hump:

$$\xi_{ps} = \xi_m T_{\text{loc}}/\sqrt{P_{\text{loc}}}.$$

Figure 4 shows the comparison between the PS emergence probability density (red dots, right axis) and the kurtosis (blue line, left axis) [the same as the one depicted in Fig 3(c)]. We found a remarkable juxtaposition of the maxima of two curves. The asymmetry of the kurtosis at its overshoot can be explained by the presence of the next steps of the Bertola-Tovbis scenario in the evolution of the partially coherent wave. Indeed, the emergence of double-peak coherent structures that follow after the local PS is obvious in the spatiotemporal diagram [Fig. 3(b)].

The possibility of predicting a position of the kurtosis maximum can be applied to different areas including fiber optics. Following Ref. [29], we provide numerical estimates of the maximum of the kurtosis for experimental parameters when the nonlinear propagation is well described by the 1D NLS equation. We consider two signals of initial spectral widths 0.1 THz and 0.2 THz with average power 2.6 W. The optical fiber has the following characteristics: $\beta_2 = -22$ ps^2/km and $\gamma = 2.4$ (Wkm)$^{-1}$. Figures 5(a) and 5(b) show dependence of the kurtosis on the propagation distance in km (left blue axis, blues curve) superimposed with the dependence of the local PS emergence probability density (right red axis, red dots). For the real parameter simulations we used a numerical box of 2^{12} points for each of 10 000 realizations. The value of nonlinearity in these two cases is less than in the one depicted in Fig. 4; the corresponding values of ϵ are 0.26 and 0.53. For random waves with larger values of ϵ only the first stage of Bertola-Tovbis scenario is regularly present in the nonlinear

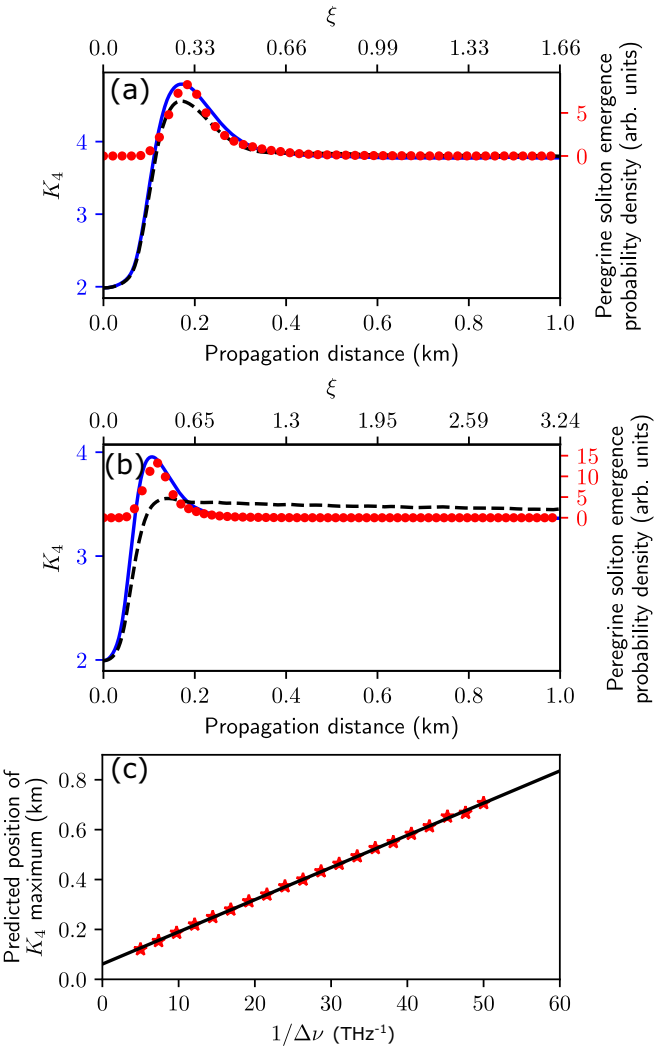

FIG. 5. Numerical simulations with real optical parameters. (a) and (b) Comparison between the probability density of local PS emergence point (red dot, right axis) and the kurtosis at different propagation distances (blue line, left axis). Black dashed line corresponds to the kurtosis of the partially coherent signal with zero phase. Spectral width of the partially coherent initial conditions 0.1 (a) and 0.2 (b) THz, average power is 2.6 W for both cases, $\beta_2 = -22$ ps^2/km, and $\gamma = 2.4$ (W km)$^{-1}$. These parameters correspond to ϵ 0.26 and 0.53, respectively. (c) Prediction for the kurtosis maximum position for different values of spectral width keeping all other parameters fixed. Covered range of ϵ varies from 0.053 to 0.53.

propagation. Therefore, the overshoot of the kurtosis is mostly given by the local PS, which also follows from the fact that the width of the overshoot coincides well with the width of the distribution of PS emergence distances.

However, considering parameters far from the semiclassical limit, we expect that the role of the nonconstant phase in partially coherent wave dynamics is increasing. This follows directly from the expressions (2). We investigate the influence of the phase by providing similar numerical simulations with exactly the same initial data $\psi(\tau, 0)$ but setting the phase in the direct space to zero so the new initial conditions are simply $|\psi(\tau, 0)|$. The evolution of K_4 in the zero phase case

is shown in Figs. 5(a) and 5(b) by the black dashed lines. For the spectral width of 0.1 THz we clearly see a smaller overshoot. The maximum of the overshoot is located at the same distance as in the case of the partially coherent wave. For the higher spectral width (0.2 THz) the maximum of the zero phase kurtosis is shifted forward. Its peak value is close to the one at the stationary state. Remarkably, the kurtosis in the zero phase case asymptotically tends to the one of the partially coherent wave at the stationary state.

Assuming the validity of our approach from the spectral width 0.2 THz and below, we provide systematic estimates of the position of the maximum of the kurtosis for the fixed value of average power 2.6 W. Figure 5(c) shows the dependence of the peak value of the kurtosis as a function of inverse spectral width. In the given range of parameters, the dependence is close to linear.

V. CONCLUSION AND DISCUSSION

We can conclude that the universal mechanism of gradient catastrophe regularization through the local formation of Peregrine soliton-like structures plays an important role in the integrable turbulence of the 1D focusing NLS equation. Its universality leads to the presence of a statistically most probable point of emergence of the PSs, which is represented by an overshoot in the kurtosis evolution.

This process can be considered as a possible explanation of the RW formation problem, of course, only at the leading order. Indeed, experimental works (see, for example, Ref. [18]) suggest that the dynamics of surface gravity waves having high values of steepness can significantly deviate from the one predicted by the NLS equation. However, the presence of overshoot in the evolution of the kurtosis is also found in nonintegrable hydrodynamic models such as the Dysthe equation or even the full Euler equations as well as real experimental data [10,56,57]. This suggests that the presented way of predicting the maximum of the kurtosis could be extended to a more general case by taking into the account the influence of higher order terms. The applicability of this approach to nonintegrable systems has to be thoughtfully analyzed, which is far beyond the scope of this article.

Part of the ideas presented in this article were proposed in the Ph.D. thesis written by the author [58].

ACKNOWLEDGMENTS

This work has been partially supported by the Agence Nationale de la Recherche through the LABEX CEMPI project (ANR-11-LABX-0007), Ministry of Higher Education and Research, Hauts-De-France Regional Council and European Regional Development Fund (ERDF) through the Contrat de Projets Etat-Region (CPER Photonics for Society Grant No. P4S). The author wants to express his gratitude to Prof. P. Suret and Prof. S. Randoux for guidance, support, and the possibility to pursue independent research. The author is grateful to Prof. G. El for very fruitful discussions. Also, the author thanks G. Michel and A. Cazaubiel for reading the draft and making useful comments.

[1] C. Kharif, E. Pelinovsky, and A. Slunyaev, *Rogue Waves in the Ocean* (Springer-Verlag, Berlin, Heidelberg, 2008).
[2] M. Onorato, S. Residori, U. Bortolozzo, A. Montina, and F. T. Arecchi, Phys. Rep. **528**, 47 (2013).
[3] D. A. G. Walker, P. H. Taylor, and R. E. Taylor, Appl. Ocean Res. **26**, 73 (2004).
[4] S. Birkholz, C. Brée, A. Demircan, and G. Steinmeyer, Phys. Rev. Lett. **114**, 213901 (2015).
[5] W. Cousins, M. Onorato, A. Chabchoub, and T. P. Sapsis, Phys. Rev. E **99**, 032201 (2019).
[6] M. Onorato, A. R. Osborne, M. Serio, L. Cavaleri, C. Brandini, and C. T. Stansberg, Phys. Rev. E **70**, 067302 (2004).
[7] K. Hasselmann, T. Barnett, E. Bouws, H. Carlson, D. Cartwright, K. Enke, J. Ewing, H. Gienapp, D. Hasselmann, P. Kruseman *et al.*, Measurements of wind-wave growth and swell decay during the Joint North Sea Wave Project (JONSWAP), Tech. Rep. (Deutches Hydrographisches Institut, 1973).
[8] M. K. Ochi, *Ocean Waves: The Stochastic Approach*, Cambridge Ocean Technology Series Vol. 6 (Cambridge University Press, Cambridge, 2005).
[9] B. Kibler, J. Fatome, C. Finot, G. Millot, F. Dias, G. Genty, N. N. Akhmediev, and J. M. Dudley, Nat. Phys **6**, 790 (2010).
[10] R. El Koussaifi, A. Tikan, A. Toffoli, S. Randoux, P. Suret, and M. Onorato, Phys. Rev. E **97**, 012208 (2018).
[11] V. E. Zakharov, J. Appl. Mech. Tech. Phys. **9**, 190 (1968).
[12] M. Onorato, A. R. Osborne, M. Serio, and S. Bertone, Phys. Rev. Lett. **86**, 5831 (2001).
[13] A. R. Osborne, *Nonlinear Ocean Waves and the Inverse Scattering Transform* (Elsevier, New York, 2002).
[14] A. Chabchoub, N. P. Hoffmann, and N. N. Akhmediev, Phys. Rev. Lett. **106**, 204502 (2011).
[15] G. P. Agrawal, *Nonlinear Fiber Optics* (Academic Press, Oxford, 2013).
[16] W. Bao, in *Dynamics in Models of Coarsening, Coagulation, Condensation and Quantization*, Vol. 9 (World Scientific, Singapore, 2007), pp. 141–240.
[17] V. E. Zakharov and A. B. Shabat, Sov. Phys. JETP **34**, 62 (1972).
[18] L. Shemer, A. Sergeeva, and A. Slunyaev, Phys. Fluids **22**, 016601 (2010).
[19] A. Chabchoub, N. Hoffmann, M. Onorato, A. Slunyaev, A. Sergeeva, E. Pelinovsky, and N. Akhmediev, Phys. Rev. E **86**, 056601 (2012).
[20] A. Slunyaev, E. Pelinovsky, A. Sergeeva, A. Chabchoub, N. Hoffmann, M. Onorato, and N. Akhmediev, Phys. Rev. E **88**, 012909 (2013).
[21] N. N. Akhmediev and V. I. Korneev, Theor. Math. Phys. **69**, 1089 (1986).
[22] E. A. Kuznetsov, Dokl. Akad. Nauk SSSR **236**, 575 (1977) [Sov. Phys. Dokl. **22**, 507 (1977)].

[23] Y. Ma, Stud. Appl. Math. **60**, 43 (1979).
[24] D. H. Peregrine, J. Aust. Math. Soc. B **25**, 16 (1983).
[25] N. N. Akhmediev, A. Ankiewicz, and M. Taki, Phys. Lett. A **373**, 675 (2009).
[26] N. Akhmediev, A. Ankiewicz, and J. M. Soto-Crespo, Phys. Rev. E **80**, 026601 (2009).
[27] V. I. Shrira and V. V. Geogjaev, J. Eng. Math. **67**, 11 (2010).
[28] J. M. Dudley, F. Dias, M. Erkintalo, and G. Genty, Nat. Photonics **8**, 755 (2014).
[29] A. Tikan, S. Bielawski, C. Szwaj, S. Randoux, and P. Suret, Nat. Photonics **12**, 228 (2018).
[30] A. Chabchoub, Phys. Rev. Lett. **117**, 144103 (2016).
[31] A. Cazaubiel, G. Michel, S. Lepot, B. Semin, S. Aumaître, M. Berhanu, F. Bonnefoy, and E. Falcon, Phys. Rev. Fluids **3**, 114802 (2018).
[32] M. Bertola and A. Tovbis, Commun. Pure Appl. Math. **66**, 678 (2013).
[33] A. Tikan, C. Billet, G. El, A. Tovbis, M. Bertola, T. Sylvestre, F. Gustave, S. Randoux, G. Genty, P. Suret, and J. M. Dudley, Phys. Rev. Lett. **119**, 033901 (2017).
[34] E. Madelung, Z. Phys. **40**, 322 (1927).
[35] G. El and M. A. Hoefer, Physica D **333**, 11 (2016).
[36] B. Dubrovin, T. Grava, and C. Klein, J. Nonlinear Sci. **19**, 57 (2009).
[37] G. Fotopoulos, D. Frantzeskakis, N. Karachalios, P. Kevrekidis, V. Koukouloyannis, and K. Vetas, Commun. Nonlinear Sci. **82**, 105058 (2020).
[38] C. Hoffmann, E. G. Charalampidis, D. J. Frantzeskakis, and P. G. Kevrekidis, Phys. Lett. A **382**, 3064 (2018).
[39] V. E. Zakharov, Stud. Appl. Math. **122**, 219 (2009).
[40] D. S. Agafontsev and V. E. Zakharov, Nonlinearity **28**, 2791 (2015).
[41] S. Toenger, T. Godin, C. Billet, F. Dias, M. Erkintalo, G. Genty, and J. M. Dudley, Sci. Rep. **5**, 10380 (2015).
[42] M. Närhi, B. Wetzel, C. Billet, S. Toenger, T. Sylvestre, J.-M. Merolla, R. Morandotti, F. Dias, G. Genty, and J. M. Dudley, Nat. Commun. **7**, 13675 (2016).
[43] A. E. Kraych, D. Agafontsev, S. Randoux, and P. Suret, Phys. Rev. Lett. **123**, 093902 (2019).
[44] P. Walczak, S. Randoux, and P. Suret, Phys. Rev. Lett. **114**, 143903 (2015).
[45] S. Randoux, P. Walczak, M. Onorato, and P. Suret, Physica D **333**, 323 (2016).
[46] P. Suret, R. E. Koussaifi, A. Tikan, C. Evain, S. Randoux, C. Szwaj, and S. Bielawski, Nat. Commun. **7**, 13136 (2016).
[47] N. N. Akhmediev, J. M. Soto-Crespo, and N. Devine, Phys. Rev. E **94**, 022212 (2016).
[48] J. M. Soto-Crespo, N. Devine, and N. Akhmediev, Phys. Rev. Lett. **116**, 103901 (2016).
[49] P. G. Grinevich and P. M. Santini, Nonlinearity **31**, 5258 (2018).
[50] P. G. Grinevich and P. M. Santini, Russ. Math. Surv. **74**, 211 (2019).
[51] P. Suret, G. El, M. Onorato, and S. Randoux, in *Nonlinear Guided Wave Optics*, Series in Emerging Technologies in Optics and Photonics, edited by S. Wabnitz (IOP Publishing, 2017), pp. 12-1–12-32.
[52] K. Henderson, D. Peregrine, and J. Dold, Wave Motion **29**, 341 (1999).
[53] G. Roberti, G. El, S. Randoux, and P. Suret, Phys. Rev. E **100**, 032212 (2019).
[54] M. Onorato, D. Proment, G. El, S. Randoux, and P. Suret, Phys. Lett. A **380**, 3173 (2016).
[55] A. Gelash, D. Agafontsev, V. Zakharov, G. El, S. Randoux, and P. Suret, Phys. Rev. Lett. **123**, 234102 (2019).
[56] M. Onorato, A. R. Osborne, M. Serio, and L. Cavaleri, Phys. Fluids **17**, 078101 (2005).
[57] L. Shemer and A. Sergeeva, J. Geophys. Res. Oceans **114**, C01015 (2009).
[58] A. Tikan, Ph.D. thesis, Université de Lille/Laboratoire PhLAM, 2018.